JOURNAL OF AIRCRAFT
Vol. 48, No. 1, January–February 2011

Optimization of Active/Passive Flow Control Parameters on Airfoils at Transonic Speeds

Y. Volkan Pehlivanoglu*
Turkish Air Force Academy, 34149 Istanbul, Turkey
and
Bedri Yagiz†
Old Dominion University, Norfolk, Virginia 23529

DOI: 10.2514/1.C031066

To improve aerodynamic performance, the active and passive flow control parameters are optimized in different combinations. The flow is simulated by solving the Navier–Stokes equations and a turbulence model. The active flow control is applied using flow suction or blowing on an airfoil, and its design variables are set to be the location and the angle of the suction/blowing port and the mass flow coefficient at this port. Airfoil surfaces are parameterized by using Bezier curves to optimize an airfoil shape in a passive way. To validate the computational methodology, successful comparisons have been made with available data. A reel coded genetic algorithm is used in all optimization processes. For the demonstration problems considered herein, the best result is provided by the sequential optimization process, which results in 575.8% increment in aerodynamic performance, 183.76% increment in lift coefficient, and 68% decrease in drag coefficient.

Nomenclature

C_D	=	drag coefficient
C_L	=	lift coefficient
C_p	=	pressure coefficient
C_q	=	mass flow coefficient
c	=	chord of the airfoil
L/D	=	lift-to-drag ratio
M_∞	=	freestream Mach number
Re_c	=	Reynolds number
x_c	=	center location of actuator
α	=	angle of attack
γ	=	actuator jet angle

I. Introduction

ENGINEERING design of an airplane wing roughly consists of three stages: conceptual design such as determining the span length, maximum thickness, taper ratio, sweep angle, and aspect ratio; preliminary design including airfoil shape and its optimization, and detailed design including the detailed plan for manufacturing of the wing. In a preliminary design phase, designers start with a good baseline design and then concentrate on improving its performance by using optimization techniques. For transonic commercial aircraft wing design, the primary goal is to improve the wing performance at the cruise conditions without severe penalty at off-design conditions. The main issue at this stage is a shock wave reduction problem. A wave drag is caused by the formation of shock waves around the wing. Shock waves radiate away a considerable amount of energy that is experienced by the aircraft as drag. The magnitude of the rise in drag is impressive, typically peaking at about four times the normal subsonic drag. As this consumes energy, it is highly beneficial to eliminate the effects of shock wave at the design phase.

Optimization is a key tool to reduce the effects of shock wave and it is heavily based on the reforming of an airfoil shape in a passive way. Since the 1970s, the use of numerical optimization techniques in airfoil and wing geometry design has received considerable attention. Both gradient-based [1,2] and nongradient-based algorithms [3,4] have been employed as a numerical optimization tool for airfoil shape design. In addition to passive flow control based on aerodynamic shape optimization techniques, active flow control (AFC) can also provide a high aerodynamic performance enhancement by optimizing its parameters. AFC has been a topic of major research in fluid mechanics for more than two decades [5]. There are numerous published studies to enable AFC benefits on airfoils at subsonic speeds [6–8]. However, there are few studies related to aerodynamic performance enhancement based on AFC at transonic speeds. Vadillo et al. showed that a small disturbance close to the shock can result in large changes in the performance of the airfoil at transonic and supersonic speeds [9]. Yagiz and Kandil [10] evaluated the capability of weakening the shock waves to improve the aerodynamic performance in transonic conditions by using surface suction/blowing on airfoils via gradient-based optimization process. They selected the suction/blowing speed and angle as design parameters keeping the locations fixed. However, AFC alone may not be sufficient to get the best designs. Therefore, it is recommended to study simultaneous AFC and passive flow control techniques.

The desired goal of the present study is to improve the aerodynamic performance on an airfoil at transonic speed by optimizing the airfoil shape and/or surface suction/blowing parameters. For this reason, four different optimization cases were studied: 1) Case I, the optimization of AFC parameters on NACA 64A010 airfoil; 2) Case II, the optimization of shape control parameters starting with NACA 64A010 baseline airfoil; 3) Case III, the simultaneous optimization of active flow and shape control parameters starting with NACA64A010 baseline airfoil; and 4) Case IV, the sequential optimization of active flow and shape control parameters starting with NACA 64A010 baseline airfoil.

For these applications, real coded genetic algorithm (GA) is used to search for the optimal design. For the flow simulations, a time-dependent, turbulent flow solver is used on structured grids. Present computations were performed for Re_c 6.07 million, M_∞ 0.85 flow past airfoil at α 1°.

II. Mathematical Model

A. Numerical Model for Flow Analysis

The thin-layer approximation to the time-dependent, conservation form of the Reynolds-averaged Navier–Stokes equations are solved

Received 12 April 2010; revision received 11 August 2010; accepted for publication 20 August 2010.

*Major, Turkish Air Force; vpehlivan@hho.edu.tr.
†Graduate Research Assistant, Aerospace Engineering Department. Student Member AIAA.

by an implicit, approximately factored, finite volume, upwind and multigrid algorithm. Because of the high Reynolds number of the flow, it was assumed to be fully turbulent. One-equation Spalart–Allmaras model was used to compute a turbulent eddy viscosity. The details of the code can be found in the reference by Krist et al. [11]. A two-level multigrid technique was used to achieve the convergence acceleration. In AFC applications, the calculation is initiated from a steady state solution obtained for the flow in the absence of any jets. Then, the control cases are started from this steady solution until the residual is driven down to 10^{-9}. The actuator is modeled as a boundary condition that computes the mass flow through a solid boundary. The mass flow coefficient given in Eq. (1) is defined as the ratio between the boundary and the freestream mass flows. First, a constant rate of change in the mass flow, C_{qu}, is established. Then, C_q is gradually increased from zero to a constant value within T_{st} (time for stable initiation) and then it is kept fixed:

$$C_q = (\rho u)/(\rho u)_\infty \qquad C_q = \int_0^{T_{\text{st}}} C_{qu}\,\mathrm{d}t \tag{1}$$

B. Numerical Model for Optimization Process

A nongradient-based optimization method, vibrational GA enhanced with neural networks, is a real coded GA [4]. Within the algorithm an initial population is generated by using a random number operator based on baseline shape or parameters. To describe the method mathematically, let S be the population size, D be the individual (or chromosome) dimension space, f be the objective function, and $\mathbf{Z}_i$ be the individual including genes, $z_{i,j}(t)$, described in t^{th} iteration:

$$\mathbf{Z}_i(t) = (z_{i,1}(t), z_{i,2}(t), \ldots, z_{i,D}(t)), \qquad z_{i,j}(t) \in R^D, \qquad |^{i=1,2,\ldots,S} \tag{2}$$

The second step is to evaluate the fitness of the current population via a defined cost function f. Then, the cost weighting fitness scaling and roulette selection procedure [12] for mating are determined. The elitism concept is applied next to ensure that the best objective function value within a population is not reduced from one generation to the next. The procedure for the elite fitness value, $f^e(t)$, and elite individual, $\mathbf{Z}^e$, is as follows:

$$f^e(t) = \underset{\mathbf{Z}_i(t)}{arg\,\min} f(t)\; and\; \mathbf{Z}^e(t) = \mathbf{Z}_i(t) \tag{3}$$

$$\mathbf{Z}^e(t) = \begin{Bmatrix} \mathbf{Z}^e(t-1), & \text{if } f^e(t) > f^e(t-1) \\ \mathbf{Z}^e(t), & \text{if } f^e(t) \le f^e(t-1) \end{Bmatrix} \tag{4}$$

The crossover technique denoted by BLX-θ [13] with $\theta = 0.5$, is applied for the new individuals. The mutation strategy is applied right after this crossover phase. At this step, there are two tools. As the first tool, the goal of the first mutation application is to provide a global random diversity in the population. For this reason, all the genes in all the chromosomes are mutated as follows:

$$z_{i,j}(t) = \begin{Bmatrix} M(z_{i,j}(t)), & \text{if } t = nf_1, n = 1, 2, \ldots \\ z_{i,j}(t), & \text{if } t \ne nf_1, n = 1, 2, \ldots \end{Bmatrix}$$
$$M(z_{i,j}(t)) = z_{i,j}(t)[1 + w_1\beta_1(1-u)]^{i=1,2,\ldots,S}_{j=1,2,\ldots,D} \tag{5}$$

where f_1 is the application frequency, β_1 is a user-defined amplitude parameter, u is a random real number between (0–1), and w_1 is a user-defined scale factor. Implementing the mutation starts from the first gene position of the first chromosome, and continues throughout the genes at the same positions in the other chromosomes. As a second tool, the goal of the second mutation application is to provide a local but controlled diversity in the population. A neural network application can be used to provide a local-controlled diversity within the population. In this application, all the genes of an elite individual are mutated as follows:

$$P_{i,j}(t) = \begin{Bmatrix} z_j^e(t)[1 + w_2\beta_2(1-u)] & \text{if } t = nf_2, n = 1, 2, \ldots \\ \phi & \text{if } t \ne nf_2 \end{Bmatrix}^{i=1,2,\ldots,N}_{j=1,2,\ldots,D} \tag{6}$$

where u is a random real number between (0–1), β_2 is a user-defined constant amplitude, and f_2 is the second application frequency. A newly generated temporal population $\boldsymbol{P}$ includes N individuals. The objective function values of this population, $\boldsymbol{f}^{\text{NN}}$, are predicted via trained neural network function, N_{func}, and the best I of them are randomly placed within the population:

$$\mathbf{f}^{\mathbf{NN}} = N_{\text{func}}(\mathbf{P}) \qquad [\mathbf{f}^{\mathbf{NN}} order] = sort(\mathbf{f}^{\mathbf{NN}})$$
$$(Z_k(t))_i = \mathbf{P}_{\mathbf{order}(i),} \,||\, {}^{k = rand[1-D]}_{i = 1, 2, ..., I} \tag{7}$$

The frequencies f_1, f_2, and I are user-defined constants. In the applications the MATLAB routine newrb is used as N_{func} [14]. After mutation operations, the new population is evaluated via the cost function, which is determined by the real flow solver. The algorithm repeats all of the preceding steps as it is necessary until the convergence criterion are satisfied. The settings for the optimizations are given in Table 1. The block diagram for the optimization process is shown in Fig. 1.

C. Design Parameters and Objective Function Description

In optimization processes there are two types of design parameters; shape parameters for airfoil forming, and flow control parameters for AFC. An airfoil can be represented using Bezier curves with a set of control points [15]. Two-dimensional Bezier curves are given by the following equations:

$$z_1(s) = \sum_{i=0}^{m} C_m^i s^i (1-s)^{m-i} z_{1,i}, \qquad i = 1, 2, \ldots, D-1 \tag{8}$$

$$z_2(s) = \sum_{i=0}^{m} C_m^i s^i (1-s)^{m-i} z_{2,i}, \qquad i = 1, 2, \ldots, D-1 \tag{9}$$

$$C_m^i = \frac{m!}{i!(m-i)!}, \qquad i = 1, 2, \ldots, D-1, \qquad m = D-1 \tag{10}$$

where s is a member of set whose values vary uniformly between [0,1]. $z_{1,i}$ and $z_{2,i}$ are the coordinates of the control points, which define the profile coordinates, $z_1(s)$ and $z_2(s)$. The two control points (0,0) and (1,0) at the leading and trailing edges are fixed. It is commonly assumed that the $z_{1,i}$ control points are fixed therefore the design parameters for forming are only the $z_{2,i}$ control points. The initial population needed for the present method is generated by using a random number operator. The number of control points is taken as 10 for upper and lower airfoil surfaces.

The following design parameters are used to parameterize the flow control: mass flow coefficient, C_q, center location of actuator, x_c, and suction/blowing angle relative to the local tangent, γ. In studied cases only one actuator is used on the upper surface and the width of the actuator, w_n, is fixed to $0.035c$. The design parameter bounds are described as follows.

Table 1 The features of GA

Symbol	Values
S/N/I	10/40/3
$f_1 - w_1 - \beta_1$	4/0.5/1
$f_2 - w_2 - \beta_2$	1/0.5/1

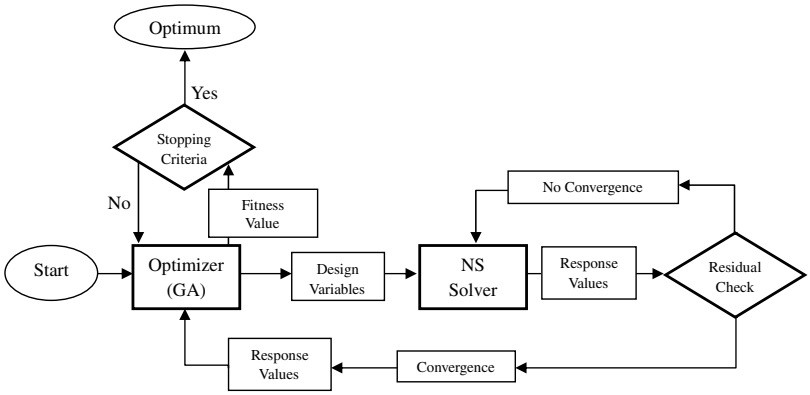

Fig. 1 Optimization process.

$$-0.2 \le C_q \le 0.025 \qquad 3^\circ \le \gamma \le 176^\circ \qquad 0.10c \le x_c \le 0.96c \tag{11}$$

Both parameter types are depicted in Fig. 2.

In shape optimization related problems, the objective function, f is to be maximized, where

$$f = \left[\frac{C_D}{C_L} + 10(C_L^* - C_{L2})^2 + 100(t^* - t)^2\right]^{-1}$$
$$C_{L2} = \begin{Bmatrix} C_L^* & \text{if } C_L \ge C_L^* \\ C_L & \text{if } C_L < C_L^* \end{Bmatrix} \tag{12}$$

C_L^* is the design lift coefficient and t^* is design maximum thickness ratio, which are taken for the demonstration case to be 0.13 and 0.1, respectively. In AFC problem, there is no need for the thickness constraint. Therefore, the objective function f is to be maximized, where

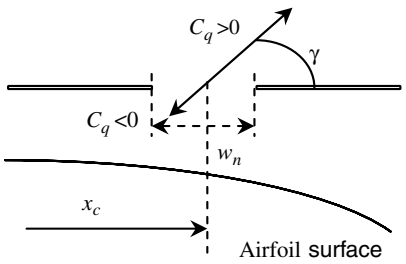

a) Active flow control parameters

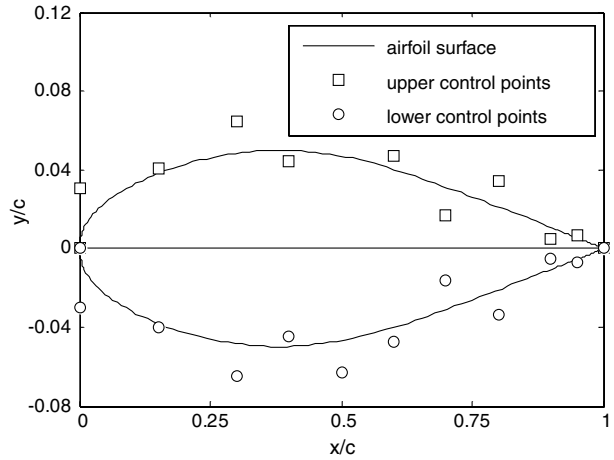

b) Shape parameters

Fig. 2 Design parameters.

$$f = \left[\frac{C_D}{C_L} + 10(C_L^* - C_{L2})^2\right]^{-1}$$
$$C_{L2} = \begin{Bmatrix} C_L^* & \text{if } C_L \ge C_L^* \\ C_L & \text{if } C_L < C_L^* \end{Bmatrix} \tag{13}$$

D. Grid Generation, Validation, and Sensitivity

Two-dimensional, 10% thick symmetric NACA64A010 was used as the test airfoil. The travel area of the actuator locations between $0.01c$ and $0.99c$ is made dense. The resolution of the utilized C-type computational grid is 449×121. Normal spacing for the first grid line of the surface of the airfoil was $0.00001c$. In the normal direction, 121 grid points were utilized with the far-field boundary located at a distance equal to 13 airfoil chord lengths. Shown in Fig. 3 are the grids used in the simulations. The grid is divided into four sub blocks to implement the parallel computing for fast computation. To demonstrate the affectivity of the present method, a solution for the airfoil without actuator was carried out. The validation case used in this study had a Reynolds number of 6.07 million based on airfoil chord, $M_\infty = 0.85$, $\alpha = 1.0^\circ$. For the preceding freestream conditions, the predicted sectional lift and drag are equal to 0.13 and 0.0329, respectively. The predicted components of airfoil drag are: 0.27338 representing the pressure component as wave drag (C_{WD}) corresponding to 83% of the total drag, and 0.00554 representing the skin friction component as form drag (C_{FD}) corresponding to 17% of the total drag. Solution sensitivity to the grid used in this study is illustrated in Table 2. For the computational cases, three sets of grids and another computational result given by Hassan et al. [16] have been used. Normalized first cell height, y^+, values, based on the height of the first wall-bounded cell, are below unity for all the meshes considered here. The solutions obtained on the course and

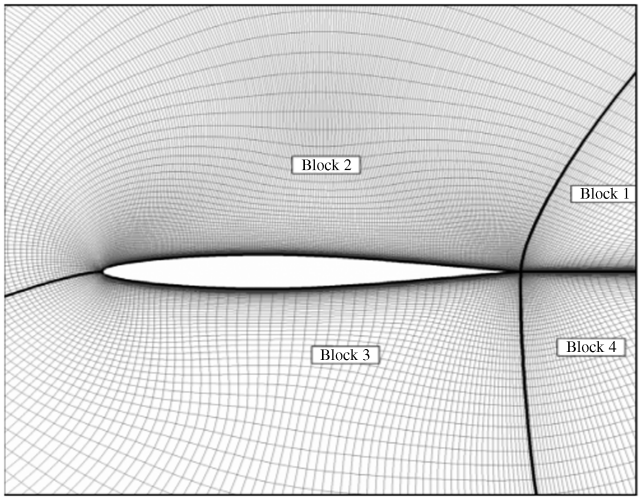

Fig. 3 Computational grid used in simulations.

Table 2 Grid sensitivity for NACA 64A010 airfoil test cases

Grid size	C_L	C_D	C_{FD}	C_{WD}
449 by 121	0.13	0.0329	0.005540	0.027338
389 by 121	0.1357	0.03233	0.00544	0.026889
281 by 99	0.1298	0.03261	0.005452	0.027158
Computation [16]	0.14	0.0328	0.00544	0.0274

fine grids are reasonably good. The results obtained on these three different grid sizes are reasonably grid-converged results and prove little solution sensitivity.

III. Optimization Results

A. Optimization of Flow Control Parameters

At first, only AFC parameters are optimized to get a maximum aerodynamic performance. The genetic optimization process takes

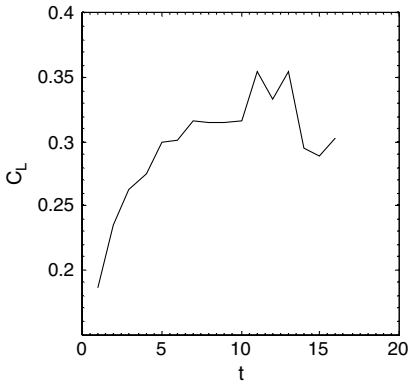

a) C_L against generations

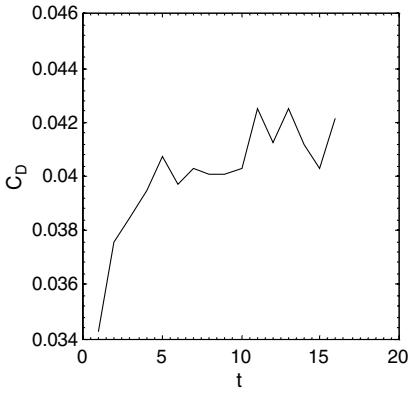

b) C_D against generations

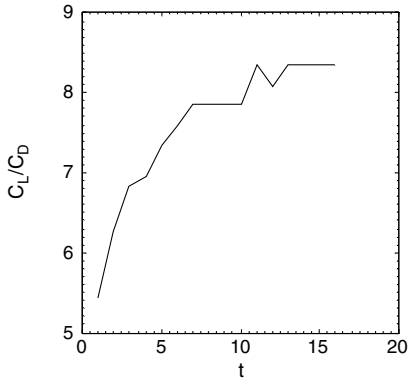

c) C_L/C_D against generations

Fig. 4 The change of aerodynamic coefficients and performance during the generations.

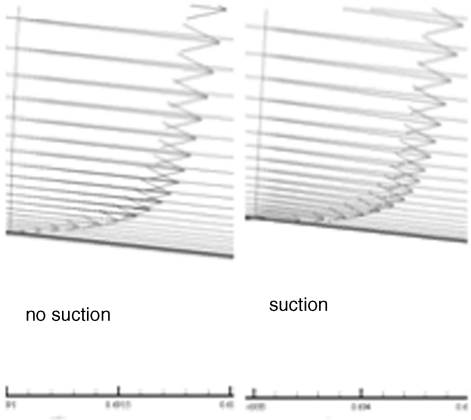

Fig. 5 Velocity profiles inside the boundary layers.

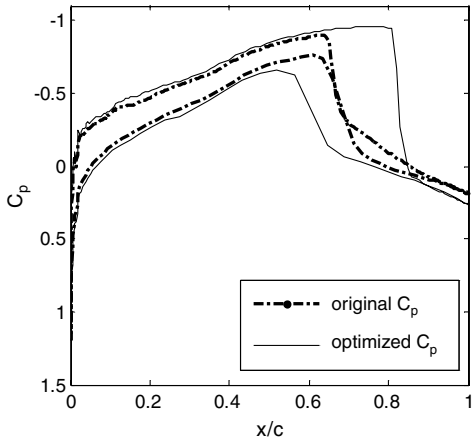

a) C_p distributions around NACA64A010

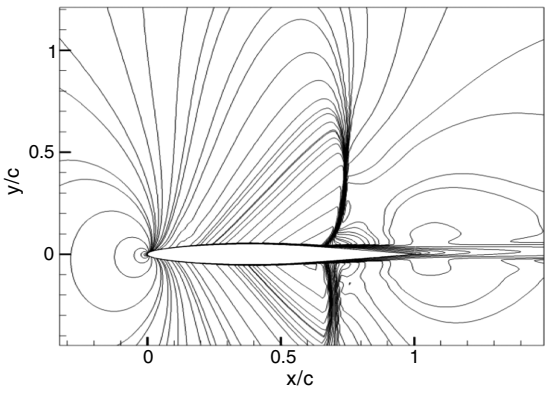

b) Mach counters around NACA64A010 without AFC

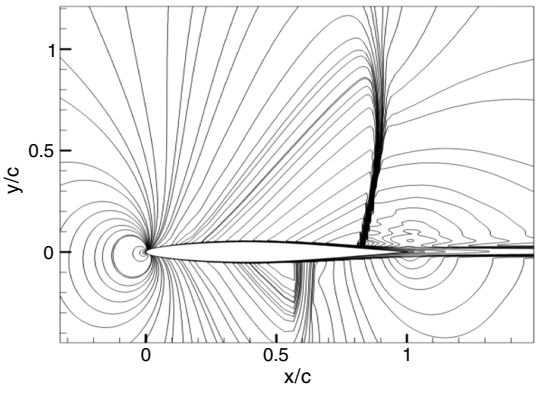

c) Mach counters around NACA64A010 with AFC

Fig. 6 C_p distributions and Mach counters around NACA64A010.

only 11 generations. At the end of the optimization process, C_q has taken the suction velocity as -0.1884, γ became the minimum angle as 3°, which is tangent to airfoil surface, and the location arrived at $0.8295c$, which is very close to shock wave location located at $0.830c$. The convergence histories of the aerodynamic coefficients, C_L, C_D, and the aerodynamic performance, C_L/C_D, are depicted in Fig. 4. After suction operation at optimal values and optimal location, C_L is increased to 0.3545, which means 272.6% increment in comparing with the original lift coefficient; on the other hand C_D is also increased to 0.04251, which means 29.17% increment in comparing with the original drag coefficient. However, the total drag increment comes from the wave drag rather than the form drag. Example velocity profiles inside the boundary layers are depicted in Fig. 5. In suction case the thickness of the boundary layer became thinner due to suction operations. As a result, the aerodynamic performance is increased to 8.339, which means 211.1% increment when compared with the original value, which is equal to 3.95.

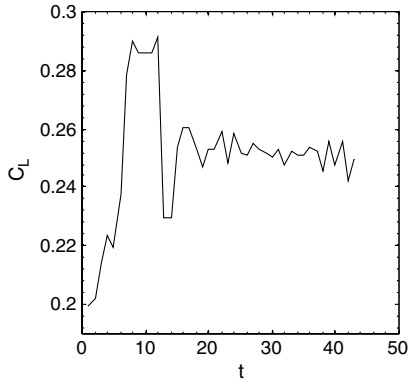

a) C_L against generations

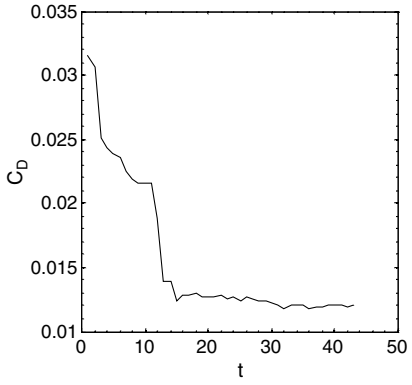

b) C_D against generations

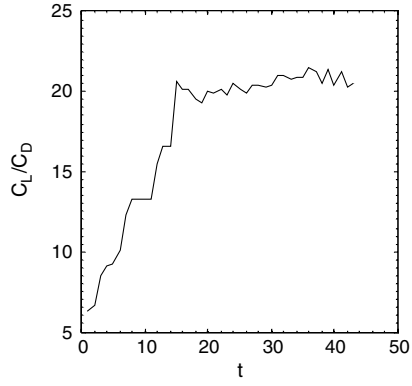

c) C_L/C_D against generations

Fig. 7 The change of aerodynamic coefficients and performance during the generations.

On the other hand, the C_p distributions and Mach counters around the airfoils are depicted in Fig. 6. According to these figures, suction operation has significant effect on the positions of both upper and lower shocks. The locations of shock waves are significantly changed. The upper shock wave moved from $0.695c$ to a new location $0.830c$. This relocation causes an extension of supersonic region and also an additional strength to the upper shock wave. The position of lower shock wave is a bit different. Instead of moving forward, it is moved backward toward $0.600c$. Additionally, the strength of lower shock wave is also decreased. The movement of upper shock toward the downstream extends the supersonic region resulting in better aerodynamic performance.

B. Optimization of Shape Control Parameters

In the second case, only the shape control parameters are optimized to get a maximum aerodynamic performance. The genetic optimization process takes 40 generations. The convergence histories of the aerodynamic coefficients, C_L, C_D, and the aerodynamic performance, C_L/C_D, are depicted in Fig. 7. After forming at optimal values, C_L is increased to 0.2496, which means 192% increment when compared with the original lift coefficient; C_D is decreased to 0.01213, which means 63.13% decrement when compared with the original drag coefficient. The total drag decrement comes from the wave drag rather than the form drag. At the end, C_{FD} takes the value of 0.0060 and C_{WD} takes the value of 0.0059, which is less than form drag. As a result, the objective function is increased to 20.58, which means 520.75% increment when compared with the original aerodynamic performance.

The resulted C_p distribution and Mach counter around the optimized airfoil are shown in Fig. 8. The maximum thickness ratio

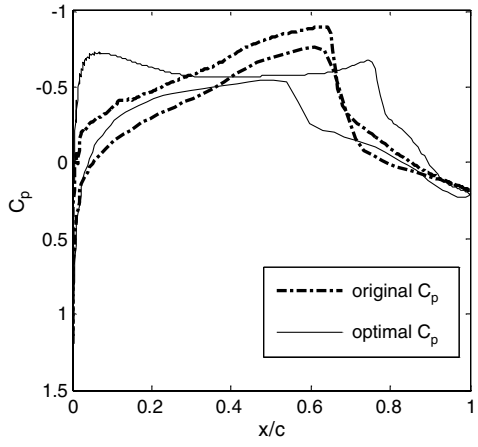

a) C_p distributions around NACA64A010 and optimized airfoil

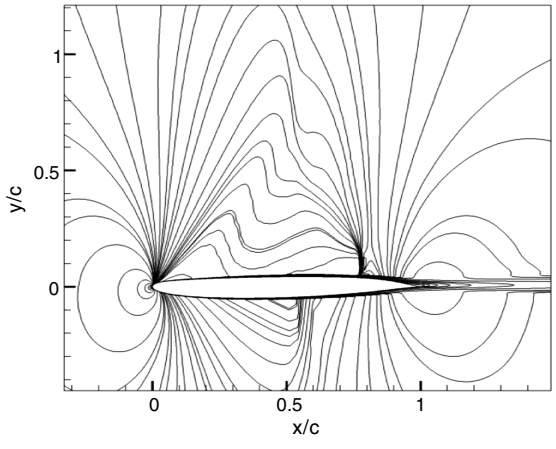

b) Mach counters around optimized airfoil shape

Fig. 8 C_p distributions and Mach counters.

for the optimal airfoil form is about 0.0963, which is good enough for the process. During the optimization, the crescent point for the upper surface moved toward the trailing edge as it is practically expected. This movement results in the relocation of the shock waves. The upper shock wave moved from the original place $0.695c$ to $0.782c$. The lower shock wave is also moved toward leading edge. Both the strengths of the shock waves are significantly decreased. However, there are still shock waves although they are weak. The main reason for the shock waves is the high freestream Mach number, which is equal to M_∞ 0.85. Practically, it is difficult to entirely eliminate the shock wave on the upper surface by using shape formation in high transonic flows.

C. Combined Optimization of Shape and Flow Control Parameters

In the third case, the shape and the flow control parameters are simultaneously optimized to get a maximum aerodynamic performance. The genetic optimization process takes about 38 generations. The convergence histories of the aerodynamic coefficients, C_L, C_D, and the aerodynamic performance, C_L/C_D, are depicted in Fig. 9. After optimization process, C_L is increased to 0.3193, which means 245.61% increment when compared with the original lift coefficient; on the other hand C_D is decreased to 0.0162, which means 50.75% decrement when compared with the original drag coefficient. As a result, the objective function is increased to 19.71, which means 498.8% increment when compared with the original aerodynamic performance.

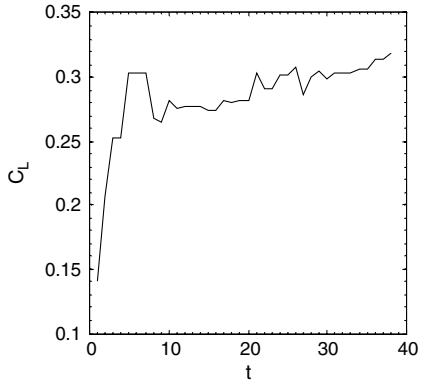

a) C_L against generations

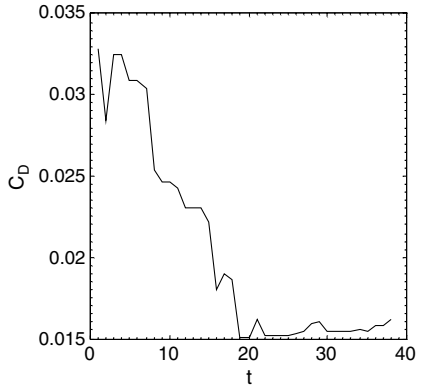

b) C_D against generations

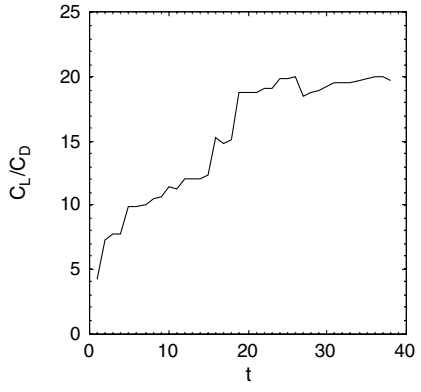

c) C_L/C_D against generations

Fig. 9 The change of aerodynamic coefficients and performance during the generations.

The resulted C_p distribution and Mach counters are shown in Fig. 10. The maximum thickness ratio for the optimal airfoil form is about 0.0881, and this result is not good enough for the process. The optimization process could not preserve the desired thickness ratio. In the objective function description given in Eq. (12) the weighting number for thickness constraint is 100 and it is good enough for this kind of problem. Because of the improper resulted shape, the second optimization process was run. In this second application the weighting number for the maximum thickness ratio is increased from 100 to 200. However, the resulted airfoil shape has 0.091 maximum thickness ratio and again it does not satisfy the required thickness ratio. From both results we understand that the main reason for the deficient thickness ratio is the AFC operations. In this optimization process, the increase in C_L originated from AFC dominates the thickness ratio constraint. It seems that AFC gives an extra thickness ratio to the airfoil shape in objective function computations. On the other hand, bigger weight number may result in insufficient design optimization space and it does not allow robust designs. Similar to previous shape optimization process, the crescent point for the upper surface moved toward the trailing edge. The upper shock wave moved from original place $0.695c$ to $0.825c$. The lower shock wave is also moved toward leading edge. Both the strengths of shock

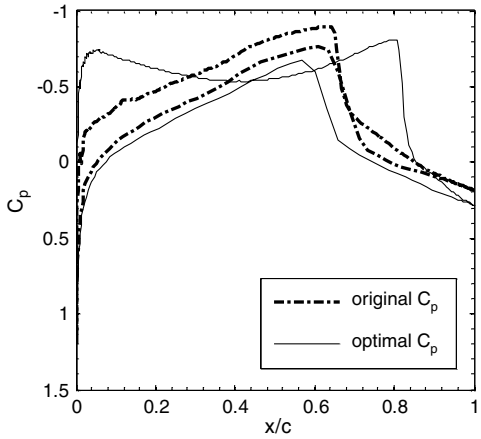

a) C_p distributions around NACA64A010 and optimized airfoil

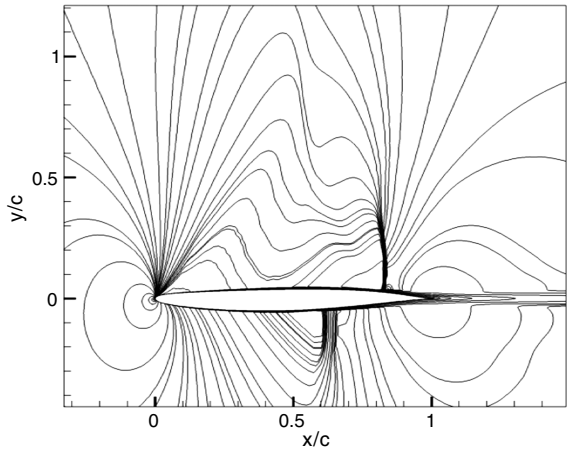

b) Mach counters around optimized airfoil shape

Fig. 10 C_p distributions and Mach counters.

waves are decreased, but there are still shock waves that cannot be ignored.

Consequently, at the end of the optimization process, C_q, has taken the suction velocity as -0.08871, γ became approximately the minimum angle as 3°, which is tangent to airfoil surface The location of actuator seems to be moved together with upper shock wave location. The upper shock is located at $0.825c$ on the optimal upper surface. The location of actuator is also located at $0.829c$, which is fairly close to the upper shock wave on the downstream.

D. Sequential Optimization of Shape and Flow Control Parameters

In the last case, the shape and flow control parameters are sequentially optimized. For this purpose the resulted shape optimized in the second case is used as a baseline airfoil form. Then, the flow control parameters are optimized on this optimal airfoil form. The genetic optimization process takes only ten generations. At the end of the optimization process, C_q, has taken the suction velocity as -0.1952, γ became approximately the minimum angle as 3°, which is tangent to airfoil surface, and the location arrived at $0.1089c$, which is close to leading edge. On the other hand, the upper shock wave located at $0.7797c$. Before the flow control operation the upper shock wave was located at $0.782c$. It seems that the suction operations get shock wave move backward. The convergence histories of the aerodynamic coefficients, C_L, C_D, and the aerodynamic performance, C_L/C_D, are depicted in Fig. 11. After suction operation at optimal values and optimal location, C_L is increased to 0.2389, which means 183.76% increment when compared with the original lift coefficient; on the other hand, C_D is decreased to 0.0105, which means 68% decrement when compared with the original drag coefficient. Interestingly, both the drag portions, the wave and the form drags, are decreased. At the end, C_{WD} takes the value of 0.0058 and C_{FD} takes the value of 0.0046, which is less than the original wave drag. As a result, the objective function is increased to 22.75, which means 575.80% increment when compared with the original aerodynamic performance. On the other hand, the suction is not located within the periphery of upper shock wave; instead, it is located within the leading-edge area. This is probably because of the eliminated shock wave. The weak shock wave causes a low level wave drag. However, the form drag is still strong. Therefore, it seems that the suction is located to decrease the form drag rather than the wave drag.

In Fig. 12 the resulted C_p distributions and Mach counters are shown. The effect of flow control operations on the pressure coefficient distributions is zoomed on the Fig. 12a. It seems it has a small scale effect. However, it causes wavy counters on Mach number distributions shown in Fig. 12b. Clearly, the optimal values provided by the sequential optimization process are so good. The sequential optimization strategy gives the best aerodynamic performance. The comparative results related to C_L, C_D, and C_L/C_D ratio are depicted in Fig. 13.

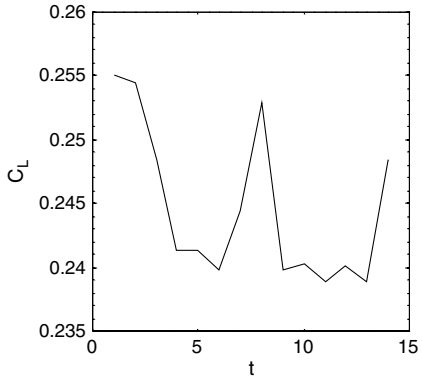

a) C_L against generations

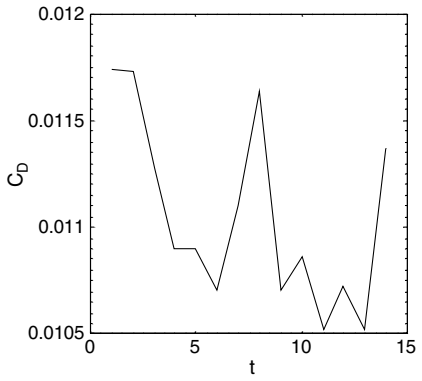

b) C_D against generations

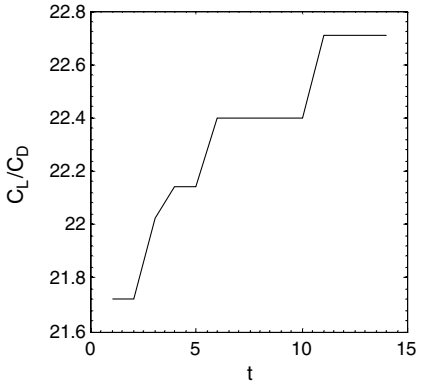

c) C_L/C_D against generations

Fig. 11 The change of aerodynamic coefficients and performance during the generations.

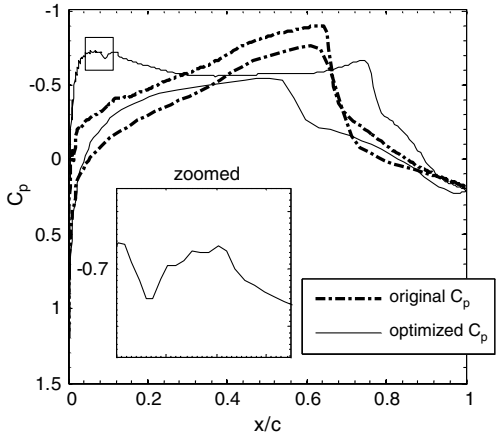

a) C_p distributions around NACA64A010 and optimized airfoil

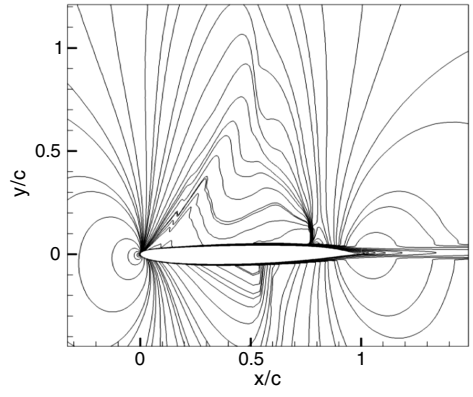

b) Mach counters around optimized airfoil shape

Fig. 12 C_p distributions and Mach counters.

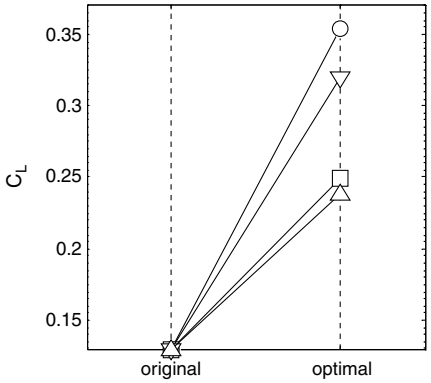

a) Comparative C_L values

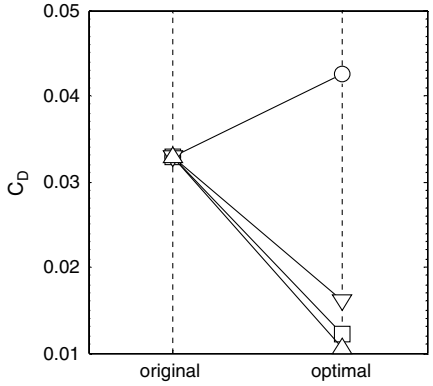

b) Comparative C_D values

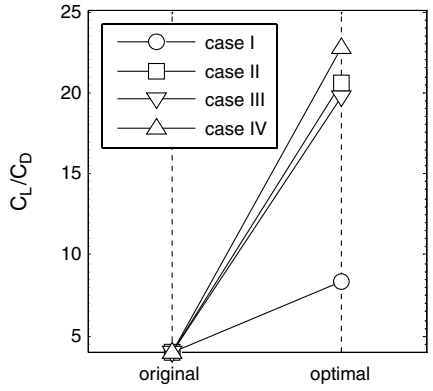

c) Comparative C_L/C_D values

Fig. 13 The comparative results among the constructed optimization cases.

IV. Conclusions

In this paper different aerodynamic optimization processes are taken into consideration. At first, only the flow control parameters on the upper surface of NACA 64A010 airfoil are optimized. At the end of the optimization process, a significant aerodynamic performance enhancement is provided. However, the main part of this success comes from the increment in C_L value rather than the decrease in C_D value. In the second case, only the shape control parameters are optimized. The current symmetric airfoil became an asymmetric, classical transonic airfoil that has almost preserved its maximum thickness ratio. The result includes a significant increase in C_L and a significant decrease in C_D.

In the third case, a simultaneous optimization process is employed. Within this study, both the flow and the shape control parameters are simultaneously optimized. The optimization resulted in 498.8% increment in aerodynamic performance when compared with the original value. However, the process cannot preserve the maximum thickness ratio constraint. It is observed that the flow control operation diminishes the effect of thickness ratio and causes a thinner airfoil. Finally, a sequential optimization process is studied. The process has given the best results including 575.8% increment in aerodynamic performance, 183.76% increment in C_L, and 68% decrease in C_D when compared with the original values.

From the results obtained, it is concluded that the optimization strategy has an important effect on the aerodynamic performance. The best way is to optimize the airfoil shape parameters at first, and then to optimize the AFC parameters.

References

[1] Leoviriyakit, K., Kim, S., and Jameson, A., "Viscous Aerodynamic Shape Optimization of Wings Including Planform Variables," AIAA Paper 2003-3498, 21st Applied Aerodynamics Conference, Orlando, FL, 23–26 June 2003.

[2] Papadimitriou, D. I., and Giannakoglou, K. C., "A Continuous Adjoint Method with Objective Function Derivatives Based on Boundary Integrals for Inviscid and Viscous Flows," *Computers and Fluids*, Vol. 36, No. 2, 2007, pp. 325–341.

[3] Hacioglu, A., and Ozkol, I., "Vibrational Genetic Algorithm as a New Concept in Aerodynamic Design," *Aircraft Engineering and Aerospace Technology*, Vol. 74, No. 3, 2002, pp. 228–236.

[4] Pehlivanoglu, Y. V., and Baysal, O., "Vibrational Genetic Algorithm Enhanced with Fuzzy Logic and Neural Network," *Aerospace Science and Technology*, Vol. 14, No. 1, 2010, pp. 56–64. doi:10.1016/j.ast.2009.11.001

[5] Gad-el-Hak, M., "Introduction to Flow Control," *Flow Control: Fundamentals and Practices*, Springer–Verlag, New York, 1998, pp. 1–108.

[6] Chang, T. L., Zhang, J., and Tsai, H. M., "A Novel Method of Flow injection and Suction for Lift Enhancement," AIAA Paper 2008-335, 46rd AIAA Aerospace Sciences Meeting and Exhibit, Reno, NV, 7–10 Jan. 2008.

[7] Duvigneau, R., and Visonneau, M., "Simulation and Optimization of Aerodynamic Stall Control Using a Synthetic Jet," AIAA Paper 2004-2315, Second AIAA Flow Control Conference, Portland, OR, 28 June–1 July 2004.

[8] Huang, L., Huang, G., and LeBeau, R., "Optimization of Airfoil Flow Control Using a Genetic Algorithm with Diversity Control," *Journal of Aircraft*, Vol. 44, No. 4, 2007, pp. 1338–1349.

[9] Vadillo, J., Agarwal, R. K., and Hassan, A. A., "Active Control of Shock/Boundary Layer Interaction in Transonic Flow over Airfoils," AIAA Paper 2005-486, 43rd AIAA Aerospace Sciences Meeting and Exhibit, Reno, NV, 10–13 Jan. 2005.

[10] Yagiz, B., and Kandil, O., "Optimization of Active Flow Control in Transonic Aerodynamics," AIAA Paper 2009-3763, 27th AIAA Applied Aerodynamics Conference, San Antonio, TX, 22–25 June 2009.

[11] Krist, S. L., Biedron, R. T., and Rumsey, C. L., "CFL3D User's Manual Version 5.0," NASA TM-1998208444, June 1998.

[12] Haupt, R. L., and Haupt, S. E., *Practical Genetic Algorithms*, 2nd ed., Wiley, Hoboken, NJ, 2004, pp. 39–40.

[13] Eshelman, L. J., and Schaffer, J. D., *Real Coded Genetic Algorithms and Interval Schemata, Foundations of Genetic Algorithms 2*, Morgan Kaufmann, San Mateo, CA, 1993, pp. 187–202.

[14] Neural Network Toolbox, MATLAB, *The Language of Technical Computing*, Ver. R2007b, The MathWorks, MA, 2007.

[15] Farin, G., *Curves and Surfaces for Computer Aided Geometric Design: A Practical Guide*, Academic Press, New York, 1993, pp. 41–42.

[16] Hassan, A. A., Osborne, B., Schwimley, S., and Billman, G., "Control of Shock-Boundary Layer Interactions (SBLIs) Using an Oscillatory Jet," AIAA Paper 2007-0476, 45th AIAA Aerospace Sciences Meeting and Exhibit, Reno, NV, 8–11 Jan. 2007.